IJE TRANSACTIONS B: Applications Vol. 33, No. 11, (November 2020) 2222-2232

International Journal of Engineering

Journal Homepage: www.ije.ir

A New Variable Frequency Zero Voltage Switching Control Method for Boost Converter Operating in Boundary Conduction Mode

S. Norouzi[a], H. Ghoreishy*[a], A. Ale Ahmad[a], F. Tahami[b]

[a] *Department of Electrical and Computer Engineering, Babol Noshirvani University of Technology, Babol, Iran*
[b] *Department of Electrical and Computer Engineering, Sharif University of Technology, Tehran, Iran*

PAPER INFO

Paper history:
Received 03 August 2020
Received in revised form 15 September 2020
Accepted 21 September 2020

Keywords:
Boundary Conduction Mode
DC-DC Gan Boost Converter
Fully Zero Voltage Switching
High Frequency Switching
Valley Switching
Extended Switching
Zero Current Switching

ABSTRACT

This paper proposes a new variable frequency zero voltage switching (ZVS) control method for boost converter operating in boundary conduction mode (BCM). The intended method keeps the converter in BCM despide of the load and input voltage variations. This is done by changing switching frequency in a certain specified range. The proposed method can guarantee circuit performance in BCM via zero-crossing detection of the inductor current and changing the switching frequency. In addition, with a slight modification in control structure, it is possible to achieve a fully ZVS in all cases. This converter control is carried out in analog form without using microprocessors which, compared with the digital one, has less noise, cost and processing challenges in high frequency applications. Simulation results obtained from applying the proposed method on a GaN-based synchronous boost converter in two different switching frequency ranges (100KHz and 1MHz) are indicative of the proposed strategy advantages.

***doi**: 10.5829/ije.2020.33.11b.14*

NOMENCLATURE

L	Inductor	Q_R	Charge for switch capacitor
D	Duty Cycle	I_L	Inductor current
V_i	Input Voltage	I_e	Extended current
V_{out}	Output Voltage	I_{em}	Negative maximum of inductor current
f_{sw}	Switching Frequency	T_R	Resonance time
C_{oss}	Switch capacitor		

1. INTRODUCTION

DC-DC boost converters are particularly significant due to their high voltage gain, input current continuity, and power factor correction. As it is known, different Pulse Width Modulation (PWM) methods are the well-known control strategies for these converters. Conventionally, in these methods, the voltage on the switch or its current is unexpectedly switched off and on, known as hard switching. Switching losses, high stresses, limitations in higher frequencies, noise amplification, and electromagnetic interferences are among the important shortcomings of hard switching. In general, to minimize the size and volume of the power electronic converters, switching frequency should be increased which, in turn, increases switching losses and Electromagnetic Interferences (EMI). To solve these issues, soft switching methods are widely employed [1, 2].

*Corresponding Author Institutional Email: *ghoreishy@nit.ac.ir* (H. Ghoreishy)

Please cite this article as: S. Norouzi, H. Ghoreishy, A. Ale Ahmad, F. Tahami, A New Variable Frequency Zero Voltage Switching Control Method for Boost Converter Operating in Boundary Conduction Mode, International Journal of Engineering (IJE), IJE TRANSACTIONS B: Applications Vol. 33, No. 11, (November 2020) 2222-2232

Soft switching techniques include Zero Current Switching (ZCS) and Zero Voltage Switching (ZVS). Using soft switching causes switching losses reduction, high efficiency, better temperature control of switches in power electronic converters [3–7].

Resonant converters are the first category of the soft switching converters. Resonance circuits are used for creating soft switching conditions in these converters. One drawback of the resonant converters is the change in structure of the converter topology where the application of passive elements in the system leads to volume and cost increment [8]. One desirable method for the realization of soft switching in DC-DC converters is converter operation in Boundary Conduction Mode (BCM); so that, unlike resonant converters, this is conducted without the slightest change in the structure of the power electronic converter. Designing in BCM mode causes reduction of the input inductor size, loss reduction of switch turn-on time and reduction of some issues regarding reverse recovery compared with design in Continuous Conduction Mode (CCM). In addition, by slightly modifying the controller, the ZVS or near ZVS (also called valley switching) can be easily achieved. Boost Power Factor Correction (PFC) converters are widely used since the switching loss of the power switch can be minimized by ZVS or valley switching [9–11].

Over the past decades, due to space limitations and issues related to weight and cost reduction, the evolution of power electronic systems tended toward systems with high energy density, leading to an efficiency increase [12–15]. High frequency Silicon switch circuits have unacceptable switching loss. Therefore, in order to obtain the appropriate voltage and current ripples, large passive elements are required. The capacitors and inductors mainly comprise a large amount of volume and area. Due to the usage of large capacitors, problems such as reduced converter efficiency and inappropriate ripple have arisen. Nevertheless, designing the converter in BCM generates more current stress, which increases switch conductive losses and size of the input filter. Wide-bandgap (WBG) switches such as SiC (Silicon carbide) and GaN (Gallium nitride) are used to solve this problem due to the low gate charge and the input and output capacitors that operate at a higher switching frequency [16–19].

Regarding properties of GaN transistors, BCM with valley switching in a boost converter was exposed as an ideal application of newly emerged GaN products. This is because the parasitic elements of the devices can be best accommodated at high frequencies i.e. losses of the devices can be minimized [20].

One of the highly significant considerations in designing circuit operation in BCM is the zero-crossing detection of the inductor current. Various methods are proposed for zero-crossing detection of the inductor current and converter operation in BCM. An inductor was used for current monitoring in [21]. Inverse current detection by a freewheeling switch was investigated and implemented in [22]. An RC filter for zero current detection was used in [23] by a series resistance in predictive online digital control method. Some sensors are employed for measuring inductor current, which are not appropriate in high frequency applications due to limitations in bandwidth, price and inaccurate current measurement. Therefore, current mirror technique, which is known as SenseFet in power electronic applications, are used for current monitoring. This technique is a simple and low-cost method with high efficiency [24, 25]. In this method, a GaN switch is used as SenseFet and the voltage drop of the sensor resistor is proportionate with switch current. Bandwidth is not limited in this method and measures current with high accuracy [26].

The BCM performance in DC-DC converters can be guaranteed by controlling the switching frequency. Regarding this matter, Variable on-time (VOT) control, which is a variable frequency technique, has been described in [27]. In this method, input voltage [28] or peak switch current [29] sampling is used to define the slope of the ramp signal, which is compared with the error amplifier output. Another method is the hysteresis control strategy in which the inductor current is limited between upper and lower bands. If the current crosses either bands, the switch control signal will be changed and the converter will remain in BCM [30].

A new method to implement ZVS in BCM with 5 MHz switching frequency is proposed in [31] which increases efficiency up to η=98%. As presented in [32, 33], having a MHz switching frequency greatly reduces size of the inductor and converter input filter that significantly affects power density of the system. Nonetheless, conditions for a fully ZVS requires input and output voltages to be within a certain range. A ZVS extension method for BCM synchronous converter is presented in [34], such that synchronous rectifier ON-time is increased in bidirectional converter; therefore, a negative inductor current, capable of discharging capacitor of the main switch, is generated. A control method for achieving ZVS is implemented in [35] by eliminating dependency to input and output ratio in a MHz BCM boost based power factor correction circuit. To obtain the negative inductor current needed for achieving ZVS, sampling of the converter input and output voltages is required [36].

All the above methods were performed assuming that the circuit remains in BCM despite the changes in input and output parameters. However, any research that covers both BCM guarantee and circuit performance in fully ZVS has not been conducted yet.

A new high frequency method for controlling boost converter in BCM is proposed in this paper. The proposed method keeps boost converter in BCM despide of load and input voltage variations by changing

switching frequency in a certain specified range. After determining the desired frequency at which the converter returns to BCM, the controller keeps the switching frequency in a projected range. The applied converter is a synchronous boost converter using WBG devices. This method can guarantee circuit performance in BCM by zero-crossing detection of the inductor current and by changing switching frequency. In addition, with a slight change in control structure, it's possible to achieve a fully ZVS in all cases. This converter control is carried out in analog form without using microprocessors which, compared with digital one, has less noise, cost and processing challenges in high frequency applications.

The basic performance of the proposed control method is discussed in Section 2; presents the BCM operation both under valley and extended ZVS. The equations that define the converter operation under these modes are presented in Section 3. The proposed self-regulating control method for ZVS extension operation is proposed in Section 4. Simulation results are examined in Section 5 to ensure the accuracy of the proposed control algorithm method.

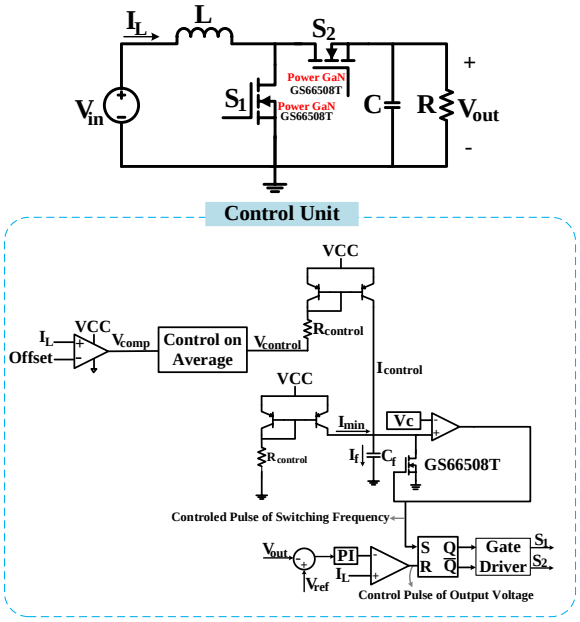

Figure 1. The boost converter and the proposed control block diagram

2. PROPOSED BOUNDRARY CONDUCTION MODE CONTROL IN A BOOST CONVERTER MODEL

The proposed BCM control method is studied in this section. In order to show the desirable performance of this technique, it is applied to a synchronous boost converter in which the diode is replaced by a power electronic switch leading to conduction loss reduction and system efficiency increase [37].

It should be noted that the proposed control method is also applicable to the conventional boost converter. On the contrary, the realization of fully ZVS occurs only when the converter diode is replaced with a synchronous switch. In order to have an integrated control strategy, both BCM control and fully ZVS realization have been applied on the synchronous boost converter.

Synchronous boost converter along with the proposed BCM control technique is shown in Figure 1.

Firstly, the boost converter is designed in BCM. Then, applying the boundary condition, inductor size is obtained via Equation (1):

$$L_{BCM} = \frac{D\,(1-D)^2 R}{2f_{sw}} \quad (1)$$

where D is the main switch duty cycle, R is the load and f_{sw} is the switching frequency. In this control method, the switching frequency varies in a pre-defined range. This range, by which the circuit can continue to operate in BCM, must first be calculated. To this end, the relationship between the input voltage, output power and output voltage variations are shown in Equation (2).

$$L_{BCM}\frac{2I_{L_{ave}}}{(V_i-\frac{V_i^2}{V_{out}})} = L_{BCM}\frac{2P_{out}}{V_i^2(1-\frac{V_i}{V_{out}})} = \frac{1}{f_{sw}} \quad (2)$$

According to Equation (2), if load current increases at the presence of the constant input and output voltages, the converter performance mode will change from BCM to CCM. The frequency variation range in which the circuit can be maintained in BCM is dependent on the input voltage, output voltage and power variations.

Figure 2 shows the frequency variations versus the input voltage and output power according to Equation (2). As can be seen from the figure, by a proper control of the switching frequency, converter can always be kept in BCM despite of the load and input voltage variations. As the output current increases, the converter performance changes from BCM to CCM.

As shown in Figure 3, the inductor current has the same mean value in both BCM and CCM operation modes. If the convertor is shifted to CCM, the control strategy can return it to BCM by reducing the frequency.

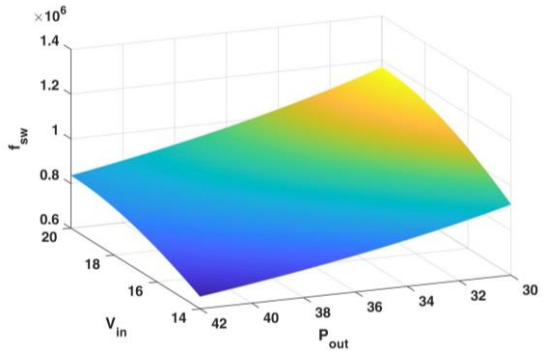

Figure 2. Frequency variation range versus input voltage and output power

In the proposed method, after inductor current sampling, an offset with a value close to zero is compared with this current. Comparator output is shown as V_{comp} in Equation (3). According to this equation, if inductor current is lower than offset value, the comparator output would be +5V.

$$V_{\text{comp}} = \begin{cases} +5 & I_L < \text{offset} \\ 0 & I_L > \text{offset} \end{cases} \quad (3)$$

where V_{comp} is a square wave. By applying this waveform to control on average block, V_{comp} average signal ($V_{control}$) is computed according to Equation (4). Then, according to Equation (5), $V_{control}$ is applied to regulate $I_{control}$. This current charges C_f and plays a crucial role in determining switching frequency of the converter.

$$V_{\text{control}} = V_{cc} - \frac{k_p \int_T V_{\text{comp}} dt}{T} \quad (4)$$

$$I_{\text{control}} = \frac{V_{cc} - V_{EB} - V_{\text{control}}}{R_{\text{control}}} \quad (5)$$

If $I_{control}$ is zero, there would be no charging source for C_f , and production of the switching frequency required for circuit performance would be disrupted. In this case, an auxiliary current source should be used to generate I_{min} for C_f charging and minimum required frequency. In general, required current for C_f charging is calculated according to Equation (6).

$$I_f = I_{\text{control}} + I_{\text{min}} \quad (6)$$

$$I_{\text{min}} = \frac{V_{cc} - V_{EB}}{R_{\text{min}}} \quad (7)$$

To discharge the capacitor, its voltage should be compared with V_c reference value. When the capacitor voltage reaches to V_c, the comparator output connected to the control switch gate is set to logic state 1. Therefore, the intended switch is turned on and the capacitor will be short-circuited. Hence, the capacitor begins to discharge. By continuous charging and discharging of the capacitor, a pulse is produced at the comparator output, the frequency of which is according to Equation (8).

$$f_{sw} = \frac{I_f}{C_f V_c} \quad (8)$$

Therefore, by applying the proposed control method, switching frequency could be regulated for circuit performance in BCM. Peak current mode method is used to stabilize the output voltage in this converter. The output pulse generated by the capacitor charging and discharging (which determines switching frequency of the converter), is inserted into a RS flip-flop set port. On the other hand, reset pulse of the intended flip-flop is applied by PI controller responsible for setting the output voltage error to zero. The flip-flop output and its complement, generate commands for S_1 and S_2 switches, respectively. In this paper, by a slight change in control structure, the condition is provided for circuit performance in fully ZVS, as discussed in the following.

3. OPERATION ANALYSIS OF BOOST CONVERTER

Inductor current in a switching interval of synchronous boost converter working in BCM is shown in Figure 4 [38].

It should be noted that given the input and output ranges and converter control method, each of these three states in Figure 4 could occur in this converter. If complete control is not applied to the converter operating in BCM, depending on the input and output ratio, modes (a) and (b) can be possible; such that in the case of $V_{in} < V_{out}$ /2, (a) and for $V_{in} > V_{out}$ /2, (b) is possible. Likewise, by appropriate control, fully ZVS can be achieved according to (c). Each switching interval includes two major times (T_{ON} and T_{OFF}) and two resonant times in all three above-mentioned states. However, all three states are similar in the first two subintervals and different in third and fourth subintervals. In the following, the first two subintervals are examined first, then three states are explained, separately.

Primary current of the inductor (I_L) and primary voltage of the capacitor of the main switch (S_1) at the beginning of each circuit switching interval is assumed as Equation (9):

$$I_L(t_0) = 0 \quad , \quad V_{DS1}(t_0) = 0 \quad (9)$$

Each switching interval of this converter is divided into four subintervals, each of which is discussed below.

Subinterval 1 [$t_0 < t < t_1$]: S_1 is turned on during this interval and inductor current increases linearly with the slope of $\frac{di}{dt} = \frac{V_{in}}{L}$. This subinterval is called turn-on time (T_{ON}), the length of which is determined by control loop of the output voltage regulation. S_1 is turned off at t_1.

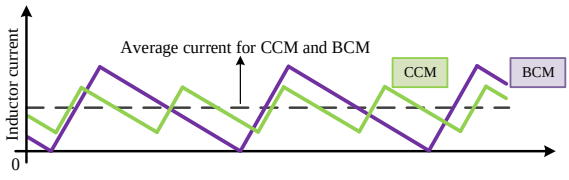

Figure 3. Inductor current in BCM and CCM modes with same mean value

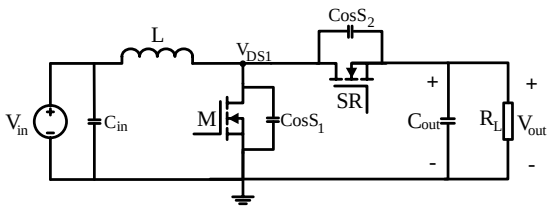

Figure 4. Synchronous boost converter

The ultimate value of I_L and V_{DS1} and length of this subinterval are as below:

$$T_{ON}=t_1-t_0 \ , \ I_L(t_1)=I_p \quad , \quad V_{DS1}(t_1)=0 \tag{10}$$

Subinterval 2 [$t_1<t<t_2$]: During this subinterval, both S_1 and S_2 are off, and a resonance occurs between the non-linear capacitors of S_1 and S_2 (C_{OSS1}, C_{OSS2}) and the inductor; therefore, C_{OSS1}, C_{OSS2} will be discharged. The length of this subinterval is short, and high inductor current is with the amount of I_P. Hence, this subinterval can be neglected for the following calculations.

The ultimate value of I_L and V_{DS1} and length of this subinterval are as below:

$$T_{R1}=t_2-t_1 \ , I_L(t_2)=I_{pp}\gg I_p \ , V_{DS1}(t_2)=V_{out} \tag{11}$$

Subinterval 3 [$t_2<t<t_3$]: When C_{OSS2} is fully discharged, diode of S_2 switch begins to flow inductor current. In fact, after a short delay (T_{R1}), S_2 switch is turned on at zero voltage. At this interval, voltage applied to the inductor is negative, thus I_L is reduced. Due to the fact that S_1 is off at this interval, this is the off-time (T_{off}).

The ultimate value of I_L and V_{DS1} and length of this subinterval are as below:

$$T_{off}=t_3-t_2 \ , \ I_L(t_3)=0 \ , \ V_{DS1}(t_2)=V_{out} \tag{12}$$

Subinterval 4 [$t_3<t<t_4$]: When I_L reaches to zero, switch S_1 is turned off and the equivalent circuit is like Figure 6; therefore, a resonance occurs between the capacitor and inductor and an oscillation with the frequency of $\omega_0 = \frac{1}{\sqrt{(L.(C_{OSS1}+C_{OSS2}))}}$ begins, the behavior of which depends on the ratio of input and output voltage, i.e. $\frac{V_{in}}{V_{out}}$.

3. 1. Natural Switching Operation ($V_{in} < \frac{V_{out}}{2}$)

When input voltage is less than $V_{out}/2$, according to Figure 5(a), V_{DS1} will be zero, and S_1 is turned on at zero voltage and negative current.

3. 2. Valley Switching Operation ($V_{in} > \frac{V_{out}}{2}$)

When input voltage is greater than $V_{out}/2$, according to Figure 5(b), V_{DS1} will be zero at resonance interval of T_{R2}, because inductor does not have enough energy to discharge capacitor and S_2 turns on at a small voltage of V_{valley}. In this case, switching loss is reduced, but fully ZVS does not occur.

The ultimate value of I_L and V_{DS1} and length of this subinterval are as below:

$$T_{off}=t_4-t_3 \ , \ I_L(t_3)=0 \ , \ V_{DS1}(t_2)=2V_{in}-V_{out}=V_{valley} \tag{13}$$

To solve this issue and achieve ZVS, S_2 should be stayed on for a longer period of time. As it can be observed in Figure 5(c), during T_{R2}, inductor current should reach to an appropriate negative current so that C_{OSS1} is fully discharged and S_1 turned on both at zero voltage and current.

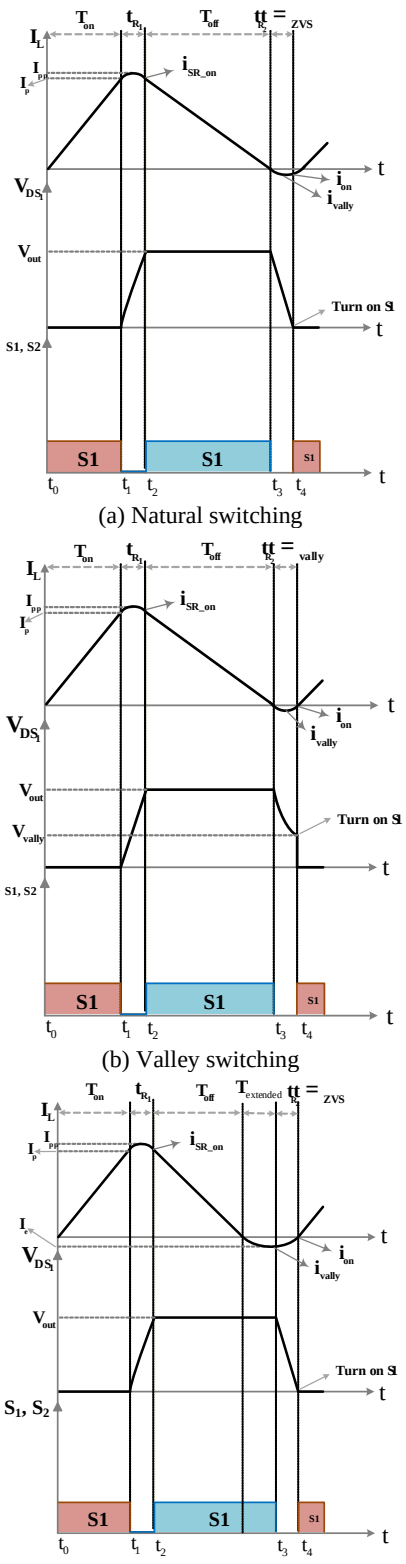

Figure 5. Current and voltage waveforms: (a) BCM natural switching operating waveforms when *Vin* ≤ 0.5*Vout*, (b) BCM valley switching operating waveforms when *Vin* > 0.5*Vout*, (c) Operation waveforms based on the proposed extended ZVS control.

4. PROPOSED ANALOG ZVS CONTROL STRATEGY

In this section, the required current (I_e) to achieve fully ZVS is calculated. Since this current depends on C_{OSS} switch capacitor and this capacitor is non-linear, according to the datasheet [39], the equationship between C_{OSS} and V_{DS} in [0-V_{OUT}] is estimated as Equation (14):

$$C_{oss} = aV_{DS}^3 + bV_{DS}^2 + cV_{DS} + d \quad (14)$$

The coefficient of a, b, c, and d are calculated using cftool software.

To achieve fully ZVS, I_L should be reduced to I_e. After reaching to I_e according to Figure 5(c), S_1 is turned off and C_{OSS1} begins to charge and C_{OSS2} begins to discharge. In this case, according to Figure 4, C_{OSS1} and C_{OSS2} are in parallel ($C = C_{oss1}||C_{oss2}$), and the equivalent circuit is according to Figure 6. Capacitor C is assumed linear and its average value is estimated as Equation (15).

$$\begin{cases} Q_R = \int_0^{V_{out}} C_{oss} dv_{DS} \\ C = C_{ave} = \frac{Q_R}{V_{out}} \end{cases} \quad (15)$$

According to Figure 7, inductor current will be as follows:

$$\begin{cases} I_L(t) = A\cos\omega_0 t + B\sin\omega_0 t + CV_{in} \\ A = I_e - CV_{in} \\ B = \sqrt{\frac{C}{L}}(V_{in} - V_{out}) \\ \omega_0 = \frac{1}{\sqrt{LC}} \end{cases} \quad (16)$$

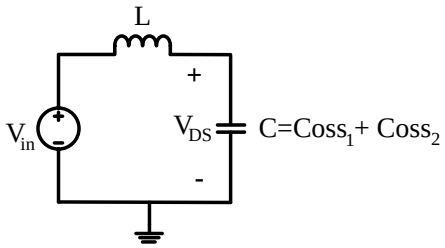

Figure 6. Equivalent resonant circuit

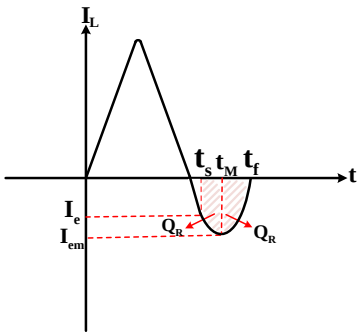

Figure 7. Detailed inductor current

To calculate I_e current, Equation (17) is used in diagram of Figure 7:

$$Q_R = \int_{t_s}^{t_m} I_L dt = \int_{t_1}^{t_2} I_L dt \quad (17)$$

In $[t_s - t_m]$, Q_R is shown as Equation (18):

$$Q_R = \frac{A}{\omega_0}\sin\omega_0 t_m - \frac{B}{\omega_0}\cos\omega_0 t_m + CV_{in} t_m + \frac{B}{\omega_0} \quad (18)$$

And in $[t_m - t_f]$:

$$Q_R = \frac{A}{\omega_0}(\sin\omega_0 t_f - \sin\omega_0 t_m) - \frac{B}{\omega_0}(\cos\omega_0 t_f - \cos\omega_0 t_m) + CV_{in}(t_f - t_m) \quad (19)$$

T_m and t_f values are calculated according to Equations (20) and (21):

$$t_m = L\frac{I_{em} - I_e}{V_{in} - V_{out}} \quad (20)$$

$$t_f = L\frac{I_{em} - I_e}{V_{in} - V_{out}} - \frac{LI_{em}}{V_{in}} \quad (21)$$

Using Equations (18)-(21) and Taylor extension, Q_R will be close to zero, I_e and I_{em} (I_{em} is the negative maximum of I_L) will be according to Equations (22) and (23):

$$\begin{cases} I_e = \sqrt{k_1^2(1-2k_2V_{out})^2 - 4(1-k_1(V_{out}-V_{in}))(k_1k_2(V_{out}+V_{in}))} \\ k_1 = \frac{Q}{L}(V_{in} - V_{out}) \\ k_2 = \frac{1}{2V_{in}} \end{cases} \quad (22)$$

$$I_{em} = \frac{k_1 + I_e^2}{I_e} \quad (23)$$

Since $T_{sw} = T_{on} + T_{off} + T_e + T_R$, each subinterval is obtained according to Equation (24):

$$\begin{cases} T_{on} = \frac{LI_m}{V_n} \\ T_{off} = \frac{LI_m}{V_o - V_n} \\ T_e = \frac{-LI_e}{V_o - V_n} \\ T_R = L\frac{I_e - I_{em}}{V_o - V_n} - \frac{LI_{em}}{V_n} \end{cases} \quad (24)$$

As stated in Section 2, the proposed closed-loop control system guarantees converter performance in BCM. Given the attained equations, fully ZVS can be obtained by a slight change in this control system. To this end, pulse commands going to S_1 and S_2 should be changed according to Figure 8. In addition, offset value computed by I_e should be replaced by Equation (22). Therefore, control loop of inductor current, in this section, determines I_e instead of zero-crossing detection. When I_L becomes equal with I_e, controlled pulse of the switching frequency goes to the R port of flip-flop2 and commands S_2 to turn off. Then, this pulse is delayed as long as T_R time span, calculated in Equation (24). C_{OSS1} is fully discharged during this time, then S_2 is commanded to be turned on. It should be noted that, as before, S_1 turn-off

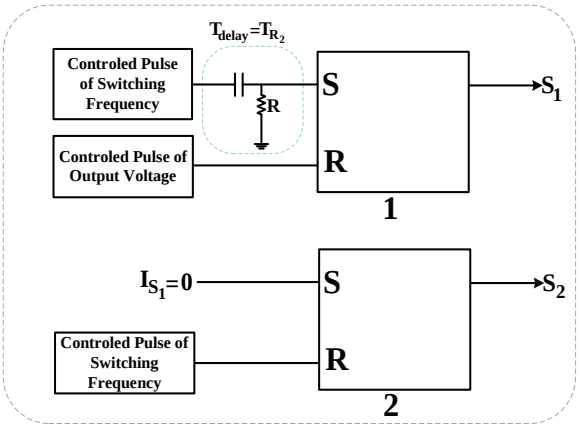

Figure 8. The simplified control diagram of the proposed system control strategy

command is issued by control loop of voltage stabilizer. To reduce the loss more than ever, turn-on command of S_2 is issued after reaching S_1 current to zero. Given the above, it is clear that the proposed control method guarantees both ZVS and ZCS.

5. SIMULATION RESULTS

In order to validate the accuracy of the circuit performance, the proposed method is applied to a synchronous boost converter and implemented in the LTspice software. Also, the values of the circuit parameters are displayed in Table 1.

Boost converter simulation is conducted by the proposed control technique in two switching frequency ranges. At first, the intended converter is simulated at 100KHz to prove the accurate performance in BCM despite load changes; then, at 1MHz switching frequency to prove that control system can achieve fully ZVS.

The steady state inductor current in BCM is shown in Figure 9(a). As can be seen from the figure, under nominal frequency and rated load, the proposed control

TABLE 1. Simulation parameters

Parameters/Devices	Symbol	Value/Number
Inductor	L	17uH(f_{sw}=100KHz) 1.7uH(f_{sw}=1MHz)
Output Capacitor	C	17.2uF(f_{sw}=100KHz) 17.2uF(f_{sw}=1MHz)
Switch	S	GS66508T
Input Voltage	V_{in}	17V
Output Voltage	V_{out}	30V
Load	R_{Load}	25Ω
Output Power	P_{out}	36W

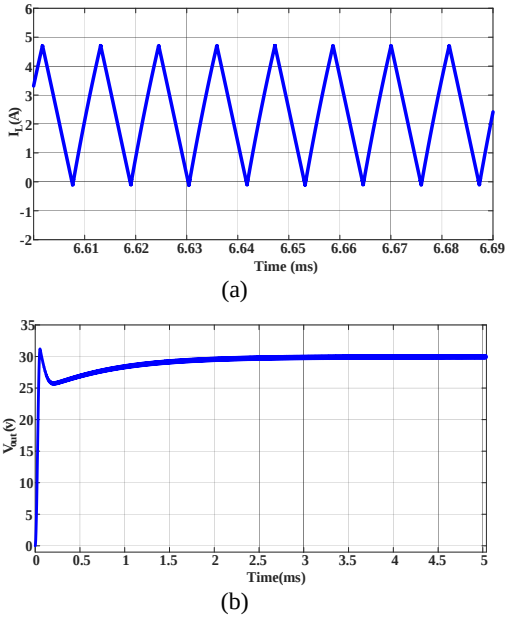

Figure 9. Simulation results: (a) Inductor current, (b) Output voltage

algorithm maintains the inductor current in BCM. Figure 9(b) shows the output voltage. As is depicted in the figure, by using the peak current mode control method, the output voltage of the circuit conforms well to its reference value. This voltage reaches to its ultimate value after 1.5ms. In this case, the load resistance and the switching frequency values are equal to 25Ω and 100 kHz respectively.

Figure 10 shows the converter output voltage at the presence of increasing the load current up to 20%. As it can be seen in Figure 10, the output voltage reaches to its reference value after 0.5ms. Moreover, due to the increase in the load current, the converter mode has changed from BCM to CCM. However, the controller performs in such a manner that the inductor current returns to BCM shortly after the load changes. The load resistance and the switching frequency values are equal to 20Ω and 80KHz respectively. It means that the controller has decreased the switching frequency in order to yield the BCM condition.

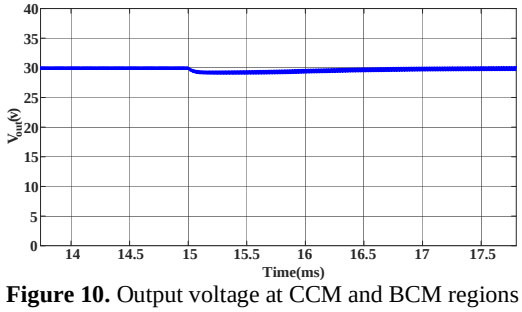

Figure 10. Output voltage at CCM and BCM regions

Figure 11 illustrates the output pulse from the comparator. According to this figure, inductor current returns from CCM to BCM after 0.5ms. As noted before, this pulse will then be entered to the averaged block.

Figure 12 shows inductor current during load current variations. As is depicted in the figure, inductor current is primarily in CCM mode. In this case, controller begins to operate and reduces the switching frequency.

Also, in Figure 13, by 20% reduction of load current, first inductor current flows from BCM to DCM; then in a short period of time (about 0.4ms), the controller

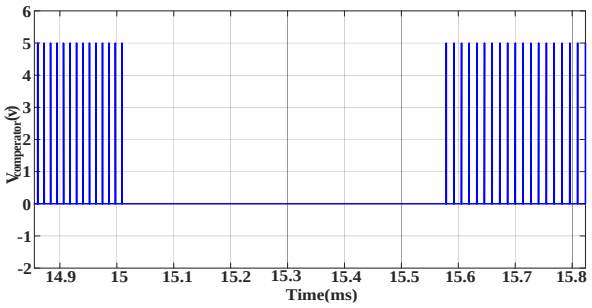

Figure 11. $V_{comparator}$ at different CCM and BCM regions

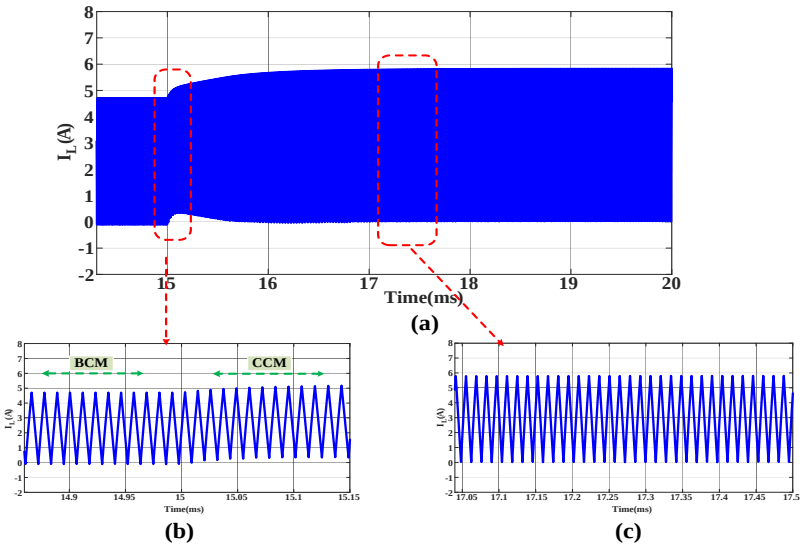

Figure 12. Inductor current at different CCM and BCM region: (a) converter operation at diffrent CCM and BCM regions, (b) inital BCM conduction (R=25Ω) and transient to CCM (R=20Ω) (First area), (c) new BCM steady-state condition after performing the control scheme (Second area)

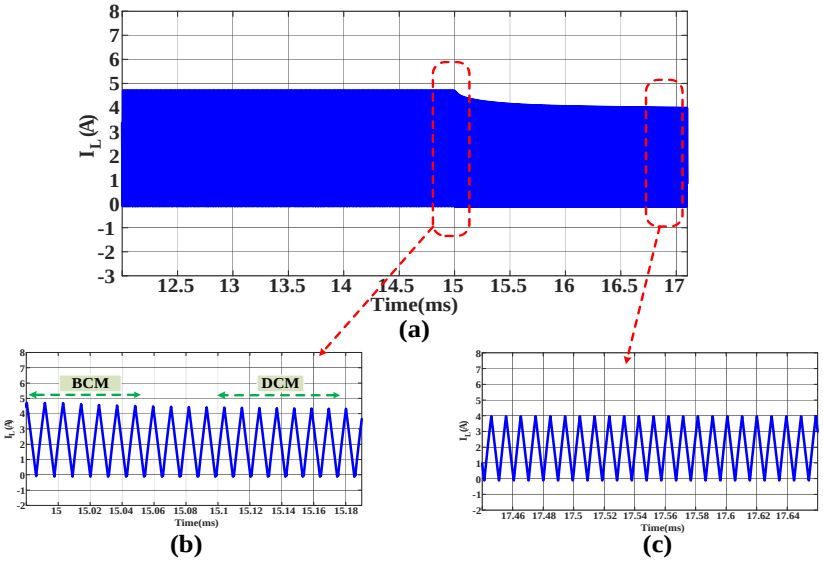

Figure 13. Inductor current at different DCM and BCM region: (a) converter operation at diffrent DCM and BCM regions, (b) inital BCM conduction (R=25Ω) and transient to DCM (R=30Ω) (First area), (c) new BCM steady-state condition after performing the control scheme (Second area)

increases switching frequency with an accurate detection of the converter performance, and converter is returned to BCM. The output voltage, in these variations, has reached to reference value in less than 0.6ms, shown in Figure 14.

In the following, simulation results of the intended converter will be examined using the proposed control method to achieve fully ZVS in 1MHz switching frequency.

Extended closed-loop control with V_{IN}, V_{OUT}, V_{DS1}, and I_L in V_{out}=30V,V_{in}=17V, f_s=1MHz to achieve fully ZVS is shown in Figure 15.

Pulse commands applied to S_1 and S_2 are shown in Figure 16. Turn-on command of S_1 is issued in ZVS and ZCS. S_1 state is "ON" during T_{on}. S_2 turn-on command will be issued when S_1 current reaches to zero. When I_L is equal to I_e (calculated in Section 4), S_2 will be turned off. Also seen in the related figure, S_1 turn-on command is delayed as much as T_R time. V_{DS1} and V_{DS2} (Figure 17) proves the accurate performance of the proposed control method.

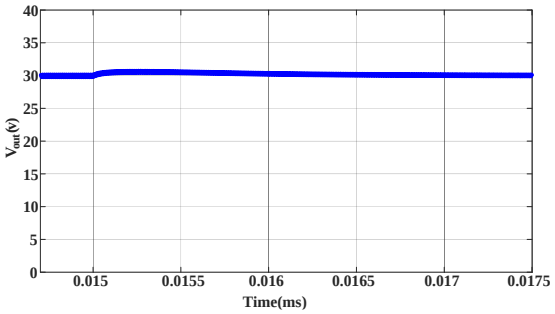

Figure 14. Output voltage at differtent DCM and BCM regions

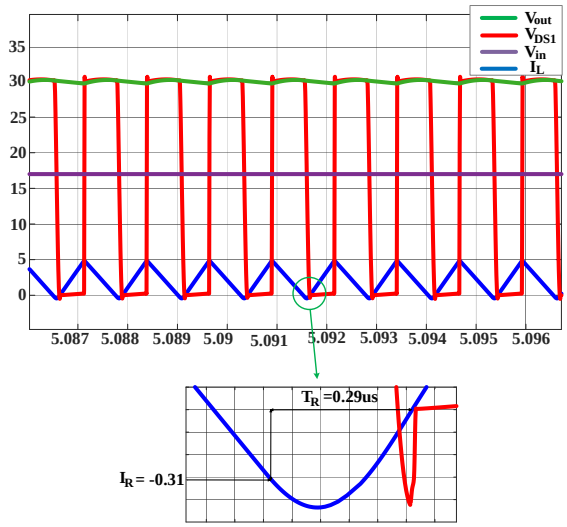

Figure 15. ZVS operation waveforms with the proposed ZVS control: Pout=36W, Vout=30V, Vin=17V, f_s =1MHz

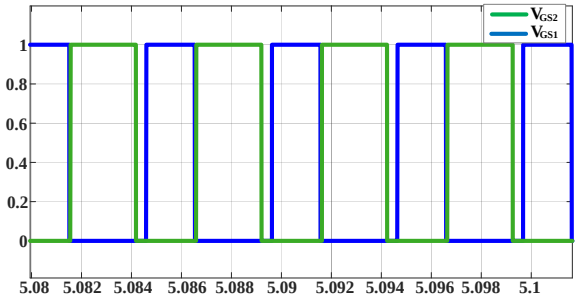

Figure 16. Pulse commands applied to S_1 and S_2

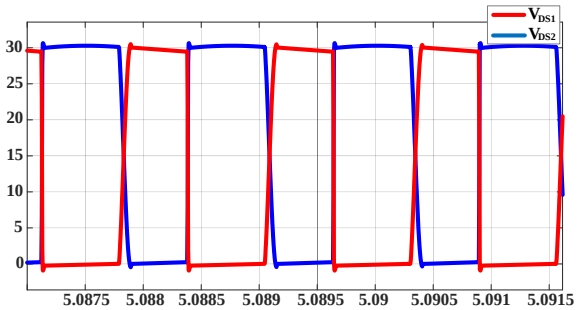

Figure 17. Zoomed in ZVS switching waveforms with improved ZVS time margin based on the proposed ZVS control

6. CONCLUSION

A new variable frequency ZVS control method for boost converter operating in BCM has been proposed in this paper. This technique is carried out in analog form without using microprocessor as analog controllers have less noise, less cost and processing problems in high frequency applications. The intended method keeps the converter in BCM in spite of load and input voltage variations by changing switching frequency in a certain specified range. In addition, with a slight change in control structure, it's possible to achieve a fully ZVS in both $V_{in}<V_{out}/2$ and $V_{in}>V_{out}/2$ cases. Simulation results obtained from applying the proposed method on a GaN-based synchronous boost converter in two different switching frequency ranges (100KHz and 1MHz) verify the proposed strategy advantages.

7. REFERENCES

1. Hariya, A., Matsuura, K., Yanagi, H., Tomioka, S., Ishizuka, Y., and Ninomiya, T. "Five-Megahertz PWM-Controlled Current-Mode Resonant DC-DC Step-Down Converter Using GaN-HEMTs." ***IEEE Transactions on Industry Applications***, Vol. 51, No. 4, (2015), 3263–3272. https://doi.org/10.1109/TIA.2015.2391439
2. Sarvi, M., Derakhshan, M., and Sedighizadeh, M. "A New

Intelligent Controller for Parallel DC/DC Converters." ***International Journal of Engineering, Transactions A: Basics***, Vol. 27, No. 1, (2014), 131–142. https://doi.org/10.5829/idosi.ije.2014.27.01a.16

3. Mohammadi, M. R., and Farzanehfard, H. "A New Family of Zero-Voltage-Transition Nonisolated Bidirectional Converters with Simple Auxiliary Circuit." ***IEEE Transactions on Industrial Electronics***, Vol. 63, No. 3, (2016), 1519–1527. https://doi.org/10.1109/TIE.2015.2498907
4. Huang, W., and Moschopoulos, G. "A new family of zero-voltage-transition PWM converters with dual active auxiliary circuits." ***IEEE Transactions on Power Electronics***, Vol. 21, No. 2, (2006), 370–379. https://doi.org/10.1109/TPEL.2005.869749
5. Zhang, Y., and Sen, P. C. "A new soft-switching technique for buck, boost, and buck-boost converters." ***IEEE Transactions on Industry Applications***, Vol. 39, No. 6, (2003), 1775–1782. https://doi.org/10.1109/TIA.2003.818964
6. Subramanian, N., Prasanth, P., Srinivasan, R., Subhesh, R. R., and Seyezhai, R. "Analysis and Experimentation of Soft Switched Interleaved Boost Converter for Photovoltaic Applications." ***International Journal of Engineering, Transactions A: Basics***, Vol. 28, No. 10, (2015), 1469–1475. https://doi.org/10.5829/idosi.ije.2015.28.10a.10
7. R, S., and Nair, M. "Simulation and Experimental Verification of Closed Loop Operation of Buck / Boost DC-DC Converter with Soft Switching." ***International Journal of Engineering, Transactions A: Basics***, Vol. 25, No. 4, (2012), 267–274. Retrieved from http://www.ije.ir/article_72033.html
8. Liu, K. H., and Lee, F. C. "Zero-voltage switching technique in DC/DC converters." In PESC Record - IEEE Annual Power Electronics Specialists Conference, (1986), 58–70. https://doi.org/10.1109/pesc.1986.7415546
9. Huber, L., Irving, B. T., and Jovanović, M. M. "Review and stability analysis of PLL-based interleaving control of DCM/ CCM boundary boost PFC converters." ***IEEE Transactions on Power Electronics***, Vol. 24, No. 8, (2009), 1992-1999. https://doi.org/10.1109/TPEL.2009.2018560
10. Husev, O., Liivik, L., Blaabjerg, F., Chub, A., Vinnikov, D., and Roasto, I. "Galvanically Isolated Quasi-Z-Source DC-DC Converter With a Novel ZVS and ZCS Technique." ***IEEE Transactions on Industrial Electronics***, Vol. 62, No. 12, (2015), 7547–7556. https://doi.org/10.1109/TIE.2015.2455522
11. Liu, Z., Huang, Z., Lee, F. C., and Li, Q. "Digital-Based Interleaving Control for GaN-Based MHz CRM Totem-Pole PFC." ***IEEE Journal of Emerging and Selected Topics in Power Electronics***, Vol. 4, No. 3, (2016), 808–814. https://doi.org/10.1109/JESTPE.2016.2571302
12. Waffler, S., and Kolar, J. W. "Efficiency optimization of an automotive multi-phase bi-directional DC-DC converter." In IEEE 6th International Power Electronics and Motion Control Conference, IPEMC '09, (2009), 566–572. https://doi.org/10.1109/IPEMC.2009.5157451
13. Hartmann, M., Miniboeck, J., Ertl, H., and Kolar, J. W. "A three-phase delta switch rectifier for use in modern aircraft." ***IEEE Transactions on Industrial Electronics***, Vol. 59, No. 9, (2012), 3635–3647. https://doi.org/10.1109/TIE.2011.2158770
14. Hartmann, M., and Kolar, J. W. "Analysis of the trade-off between input current quality and efficiency of high switching frequency PWM rectifiers." In International Power Electronics Conference - ECCE Asia -, IPEC 2010, (2010), 534–541. https://doi.org/10.1109/IPEC.2010.5543283
15. Badstuebner, U., Biela, J., Christen, D., and Kolar, J. W. "Optimization of a 5-kW telecom phase-shift dc-dc converter with magnetically integrated current doubler." ***IEEE Transactions on Industrial Electronics***, Vol. 58, No. 10, (2011), 4736–4745. https://doi.org/10.1109/TIE.2010.2103536
16. Nussbaumer, T., Raggl, K., and Kolar, J. W. "Design guidelines for interleaved single-phase boost PFC circuits." ***IEEE Transactions on Industrial Electronics***, Vol. 56, No. 7, (2009), 2559–2573. https://doi.org/10.1109/TIE.2009.2020073
17. Wang, Z., Wang, S., Kong, P., and Lee, F. C. "DM EMI noise prediction for constant on-time, critical mode power factor correction converters." ***IEEE Transactions on Power Electronics***, Vol. 27, No. 7, (2012), 3150–3157. https://doi.org/10.1109/TPEL.2011.2182059
18. Hernandez, J. C., Mira, M. C., Petersen, L. P., Andersen, M. A. E., and Petersen, N. H. "Zero Voltage Switching Control Method for MHz Boundary Conduction Mode Converters." ***IEEE Transactions on Industrial Electronics***, Vol. 67, No. 2, (2020), 1544–1554. https://doi.org/10.1109/TIE.2019.2926039
19. Zhang, Y., Yao, C., Zhang, X., Chen, H., Li, H., and Wang, J. "Power Loss Model for GaN-Based MHz Critical Conduction Mode Power Factor Correction Circuits." ***IEEE Journal of Emerging and Selected Topics in Power Electronics***, Vol. 8, No. 1, (2020), 141–151. https://doi.org/10.1109/JESTPE.2019.2948148
20. Wang, W., Pansier, F., Popovic, J., and Ferreira, J. A. "Design and optimization of a GaN GIT based PFC boost converter." ***Chinese Journal of Electrical Engineering***, Vol. 3, No. 3, (2019), 34–43. https://doi.org/10.23919/cjee.2017.8250422
21. Choi, H. "Interleaved boundary conduction mode (BCM) buck power factor correction (PFC) converter." ***IEEE Transactions on Power Electronics***, Vol. 28, No. 6, (2013), 2629–2634. https://doi.org/10.1109/TPEL.2012.2222930
22. Gao, Y., Wang, S., Li, H., Chen, L., Fan, S., and Geng, L. "A novel zero-current-detector for DCM operation in synchronous converter." In IEEE International Symposium on Industrial Electronics, (2012), 99–104. https://doi.org/10.1109/ISIE.2012.6237066
23. Chang, Y. T., and Lai, Y. S. "Online parameter tuning technique for predictive current-mode control operating in boundary conduction mode." ***IEEE Transactions on Industrial Electronics***, Vol. 56, No. 8, (2009), 3214–3221. https://doi.org/10.1109/TIE.2009.2024651
24. Liu, P., Zhang, L., Huang, A. Q., Guo, S., and Lei, Y. "High bandwidth current sensing of SiC MOSFET with a Si current mirror." In WiPDA 2016 - 4th IEEE Workshop on Wide Bandgap Power Devices and Applications, (2016), 200–203. https://doi.org/10.1109/WiPDA.2016.7799937
25. Wen, Y., Rose, M., Fernandes, R., Van Otten, R., Bergveld, H. J., and Trescases, O. "A Dual-Mode Driver IC with Monolithic Negative Drive-Voltage Capability and Digital Current-Mode Controller for Depletion-Mode GaN HEMT." ***IEEE Transactions on Power Electronics***, Vol. 32, No. 1, (2017), 423–432. https://doi.org/10.1109/TPEL.2016.2537002
26. Biglarbegian, M., Kim, N., and Parkhideh, B. "Boundary Conduction Mode Control of a Boost Converter with Active Switch Current-Mirroring Sensing." ***IEEE Transactions on Power Electronics***, Vol. 33, No. 1, (2018), 32–36. https://doi.org/10.1109/TPEL.2017.2716934
27. Ren, X., Zhou, Y., Guo, Z., Wu, Y., Zhang, Z., and Chen, Q. "Simple Analog-Based Accurate Variable On-time Control for Critical Conduction Mode Boost Power Factor Correction Converters." ***IEEE Journal of Emerging and Selected Topics in Power Electronics***, Vol. 8, No. 4, (2019), 4025-4036. https://doi.org/10.1109/JESTPE.2019.2926794
28. Kim, J. W., Choi, S. M., and Kim, K. T. "Variable on-time control of the critical conduction mode boost power factor correction converter to improve zero-crossing distortion." In Proceedings of the International Conference on Power Electronics and Drive Systems (Vol. 2), (2005), 1542–1546. https://doi.org/10.1109/peds.2005.1619933

29. Tsai, J. C., Chen, C. L., Chen, Y. T., Ni, C. L., Chen, C. Y., and Chen, K. H. "Perturbation on-time (POT) technique in power factor correction (PFC) controller for low total harmonic distortion and high power factor." ***IEEE Transactions on Power Electronics***, Vol. 28, No. 1, (2013), 199–212. https://doi.org/10.1109/TPEL.2012.2195333

30. Hariharan, K., and Kapat, S. "Need for variable frequency control in DC-DC switching converters - Challenges and opportunities using digital implementation." ***Proceedings of the Indian National Science Academy***, Vol. 84, No. 3, (2018), 657–668. https://doi.org/10.16943/ptinsa/2018/49334

31. Huang, X., Liu, Z., Lee, F. C., and Li, Q. "Characterization and enhancement of high-voltage cascode GaN devices." ***IEEE Transactions on Electron Devices***, Vol. 62, No. 2, (2015), 270–277. https://doi.org/10.1109/TED.2014.2358534

32. Hernandez, J. C., Petersen, L. P., and Andersen, M. A. E. "Characterization and evaluation of 600 v range devices for active power factor correction in boundary and continuous conduction modes." In Conference Proceedings - IEEE Applied Power Electronics Conference and Exposition - APEC, (2015), 1911–1916. https://doi.org/10.1109/APEC.2015.7104607

33. Hernandez, J. C., Petersen, L. P., and Andersen, M. A. E. "A comparison between boundary and continuous conduction modes in single phase PFC using 600V range devices." In Proceedings of the International Conference on Power Electronics and Drive Systems, (2015), 1019–1023. https://doi.org/10.1109/PEDS.2015.7203487

34. Su, B., Zhang, J., and Lu, Z. "Totem-pole boost bridgeless PFC rectifier with simple zero-current detection and full-range ZVS operating at the boundary of DCM/CCM." ***IEEE Transactions on Power Electronics***, Vol. 26, No. 2, (2011), 427–435. https://doi.org/10.1109/TPEL.2010.2059046

35. Liu, Z., Huang, X., Mu, M., Yang, Y., Lee, F. C., and Li, Q. "Design and evaluation of gan-based dual-phase interleaved MHz critical mode PFC converter." In IEEE Energy Conversion Congress and Exposition, ECCE, (2014), 611–616. https://doi.org/10.1109/ECCE.2014.6953451

36. Marxgut, C., Krismer, F., Bortis, D., and Kolar, J. W. "Ultraflat interleaved triangular current mode (TCM) single-phase PFC rectifier." ***IEEE Transactions on Power Electronics***, Vol. 29, No. 2, (2014), 873–882. https://doi.org/10.1109/TPEL.2013.2258941

37. Chen, Y., Asadi, P., and Parto, P. "Comparative analysis of power stage losses for synchronous buck converter in diode emulation mode vs. continuous conduction mode at light load condition." In Conference Proceedings - IEEE Applied Power Electronics Conference and Exposition - APEC, (2010), 1578–1583. https://doi.org/10.1109/APEC.2010.5433442

38. Huber, L., Irving, B. T., and Jovanović, M. M. "Effect of valley switching and switching-frequency limitation on line-current distortions of DCM/CCM boundary boost PFC converters." ***IEEE Transactions on Power Electronics***, Vol. 24, No. 2, (2009), 339–347. https://doi.org/10.1109/TPEL.2008.2006053

39. GaN Systems, "GS66508T, Top-side cooled 650 V E-mode GaN transistor datasheet", GaN-on silicon power transistor, (2009), 1-37.

Persian Abstract

چکیده

در این مقاله یک روش کنترلی فرکانس متغیر از کلیدزنی در ولتاژ صفر برای مبدل بوستی که در مد هدایت مرزی کار می‌کنند، پیشنهاد گردیده است. روش مذکور قادر است علیرغم تغییرات بار و ولتاژ ورودی، مبدل را از طریق تغییر فرکانس کلیدزنی در یک محدوده معین، همواره در مد هدایت مرزی نگاه دارد. تضمین باقی ماندن در این مد، با تشخیص لحظه گذر از صفر جریان سلف و تغییر فرکانس کلیدزنی امکان‌پذیر است. علاوه بر آن، با تغییر مختصری در ساختار کنترلی، دستیابی به کلیدزنی در ولتاژ صفر به طور کامل محقق می‌گردد. کنترل این مبدل به صورت آنالوگ و بدون استفاده از میکروپروسسور می‌باشد که در مقایسه با کنترل‌کننده‌های دیجیتال، دارای نویز کمتر، هزینه و چالش‌های پردازشی کمتری در کاربردهای فرکانس بالا است. نتایج شبیه‌سازی حاصل از اعمال روش پیشنهادی بر روی یک مبدل بوست سنکرون بر مبنای کلیدهای فرکانس بالای GaN، در دو محدوده متفاوت از فرکانس کلیدزنی (۱۰۰ کیلوهرتز و ۱ مگاهرتز) تاییدکننده مزایای استراتژی مذکور می‌باشد.